Supporting information

High temperature reductive treatment promotes thermal stability of Pt/hexaaluminate catalysts for CO and C_3H_8 oxidation

Yumeng Xu, [a] Rongzhou Chen, [a] Hailian Tang, [b] Lu Yan, [a] Fei Huang, *[a] Ming Tian, [c] Kaibao Wu, [a] Yanliang Zhou, [d] Jian Lin, *[c] Ying Zheng, [a] and Xiaodong Wang *[c]

[a] Fujian Provincial Key Laboratory of Advanced Materials Oriented Chemical Engineering, Fujian Provincial Key Laboratory of Polymer Materials, College of Chemistry and Materials Science, Fujian Normal University, Fuzhou 350007, Fujian, China.

[b] School of Chemistry and Chemical Engineering, Tianjin University of Technology, Tianjin 300384, China.

[c] CAS Key Laboratory of Science and Technology on Applied Catalysis, Dalian Institute of Chemical Physics, Chinese Academy of Sciences, Dalian 116023, Liaoning, China.

[d] National Engineering Research Center of Chemical Fertilizer Catalyst, Fuzhou University, Fuzhou 350002, Fujian, China.

* Corresponding author. Fax: +86 0591 83464353.

E-mail: feihuang@fjnu.edu.cn (F. H); jianlin@dicp.ac.cn (J. L) ; xdwang@dicp.ac.cn (X. W)

1. Experimental details

1.1 Preparation of hexaaluminate supports.

Hexaaluminates ($BaFe_xAl_{12-x}O_{19}$, x = 0, 1) were prepared via a $(NH_4)_2CO_3$ coprecipitation method reported in our previous work.[1] Taking $BaFeAl_{11}O_{19}$ as an example, calculated amounts of $Ba(NO_3)_2$, $Fe(NO_3)_3 \cdot 9H_2O$, and $Al(NO_3)_3 \cdot 9H_2O$ were dissolved individually in deionized water at 60 °C and then added to a saturated aqueous solution of $(NH_4)_2CO_3$ under stirring for 3 h. The resulting precipitate was filtered, washed with deionized water, and then dried at 110 °C overnight. Finally, the sample was calcined in air at 500 °C for 5 h and then 1300 °C for 6 h. The obtained $BaAl_{12}O_{19}$ and $BaFeAl_{11}O_{19}$ supports were denoted as BA and BFA, respectively. The $BaFeAl_{11}O_{19}$ precipitate precursor calcined at 900 °C for 5 h was denoted as BFA-P.

1.2 Preparation of platinum/hexaaluminate.

A facile adsorption method was employed to synthesize hexaaluminate-supported platinum catalyst. Taking the preparation of 1wt % Pt/BFA for example, 1g of BFA support was firstly dispersed in 100 mL of deionized water under ultrasonic treatment for 5 min. After that, the desired amount of K_2PtCl_4 solution was gradually dropped into the above solution, followed that the suspension was continuously stirring at room temperature overnight. The resulting precipitate was filtered, washed with 1 L of distilled water, and then dried at 80 °C overnight.

1.3 Activity measurement.

The CO oxidation (or C_3H_8 oxidation) was performed on a fixed-bed reactor and approximately 50 mg of catalyst was loaded into a U-type quartz tube for the reaction. The feed gases consisted of 1 vol% CO + 1 vol% O_2 + 98 vol% Ar (or 0.2 vol% C_3H_8 + 2 vol% O_2+ 97.8 vol% Ar). The gas flow rate was 16.67 mL min^{-1} (or 33.33 mL min^{-1} for C_3H_8 oxidation), leading to a space velocity of 20 000 mL h^{-1} g_{cat}^{-1} (or 40 000

mL h^{-1} g_{cat}^{-1} for C_3H_8 oxidation). Before evaluation, the catalyst was pre-reduced at 400 °C for 1 h in a flow of 33.33 mL min^{-1} under H_2 atmosphere. The concentrations of CO, C_3H_8, CO_2 and O_2 in the effluent gas were analyzed by an on-line gas chromatograph (PANNA A60, 5A column + Porapak Q column) using Ar as the carrier gas.

The CO conversion (or C_3H_8 conversion) was calculated using the following equation:

$$X_{[C]} = \frac{[C]_{in} - [C]_{out}}{[C]_{in}} \times 100\%$$

where C represents the CO or C_3H_8, $X_{[C]}$ represents the CO/C_3H_8 conversion. $[C]_{in}$, $[C]_{out}$ are the concentrations of CO/C_3H_8 at the inlet and outlet of the reactor, respectively.

Kinetic studies were conducted at low CO/C_3H_8 conversion levels (through adjusting the WHSV and/or feed gas composition to restrict the CO/propane conversion in a range between 4% and 15%.) to ensure differential reaction mode. *(1) apparent activation energy*: The apparent activation energy (Ea) of catalyst was obtained by studying the catalytic activity at different reaction temperatures (CO oxidation:(Pt/BFA-8O: 120 ºC - 135 ºC; Pt/BFA-8H: 30 ºC - 45 ºC) and Pt/BFA-8HO: 70 ºC - 85 ºC; C_3H_8 oxidation: Pt/BFA-8H: 190 - 265 ºC; Pt/BFA-8O and Pt/BFA-8HO: 100 ºC - 175 ºC). (a) CO oxidation: 50 mg of catalyst diluted by 500 mg of quartz was loaded in reactor and CO mixture gas (1 vol% CO+1 vol% O_2 +98 vol% Ar) was flowed (16.67 mL min^{-1}) with a mass space velocity of 20,000 mL g^{-1} h^{-1}. (b) C_3H_8 oxidation: 50 mg of catalyst diluted by 500 mg of quartz was loaded in reactor and C_3H_8 mixture gas (0.2 vol% C_3H_8+2 vol% O_2 +97.8 vol% Ar) was flowed (33.34 mL min^{-1}) with a mass space velocity of 40,000 mL g^{-1} h^{-1}. Before measurement, catalysts except the reduced ones were pre-reduced with H_2 at 400 ºC for 1h. *(2) reaction orders*: (a) CO oxidation reaction: in typical, 50 mg of catalyst diluted by 500 mg of quartz was loaded in the reactor and CO mixture gas was flowed (16.67 mL min^{-1}) with a mass space velocity of 20,000 mL g^{-1} h^{-1} at 40 ºC. The partial pressures of CO were controlled in the range of 0.5 - 2 kPa while those of O_2

were controlled in the range of 0.5 - 2 kPa. (b) C_3H_8 reaction: 50 mg of catalyst diluted by 500 mg of quartz was loaded in the reactor and C_3H_8 mixture gas was flowed (33.34 mL min^{-1}) with a mass space velocity of 40,000 mL g^{-1} h^{-1} at 220 ^oC. The partial pressures of propane were controlled in the range of 0.16 - 0.22 kPa while those of oxygen were controlled in the range of 2.0 - 2.6kPa.

2. Catalyst characterization.

X-ray diffraction (XRD) patterns were measured on a Philips X' Pert PRO MPD diffractometer equipped with a Cu Kα radiation source (λ = 0.15406 nm), operating at 40 kV and 40 mA. A continuous mode was used for collecting data in the 2θ range from 10° to 80° at a rate of 12° min^{-1} and step size of 0.0334^o.

The Pt loading over catalysts was determined by the inductively coupled plasma optical emission spectrometer (ICP-OES) on Agilent 5110.

Brunauer-Emmett-Teller (BET) surface areas of the catalysts were measured by nitrogen adsorption at -196 ^oC using a Micromeritics ASAP 2460 apparatus. The samples were outgassed to 0.1 Pa at 300 ^oC at least 3 h.

High-angle annular dark-field (HAADF) scanning transmission electron microscopy (STEM) and high-resolution transmission electron microscopy (HRTEM) Images were performed on JEOL JEF-F200 to acquire the morphologies and particle size distributions of catalysts. The powder of Pt catalyst was suspended in ethanol with an ultrasonic dispersion for 10 min and then a drop of the resulting solution was dropped on a holey carbon film supported by a copper TEM grid.

X-ray photoelectron spectra (XPS) were obtained with a Thermo Scientific K-Alpha equipment with Al Kα X-ray radiation (hν =1486.6 eV). The Pt(4d), Fe(2p) and O(1s) binding energy was calibrated with the value of contaminated carbon (C1s peak at 284.8 eV).

The ^{57}Fe Mössbauer spectra were recorded at room temperature with a spectrometer working in constant

acceleration mode with the ^{57}Co γ-quantum source in a Rh matrix. The powder samples used approximately 10 mg cm^{-2} of natural iron. All spectra were fitted by the MossWinn package, and the isomer shifts (IS) were given relative to the centroid of α-Fe at room temperature.

Temperature-programmed reduction of H_2 (H_2-TPR) was conducted on a Micromeritics Autochem 2720 instrument with a thermal conductivity detector (TCD). 100 mg of the samples were pretreated in Ar (30 mL min^{-1}) at 120 °C for 1 h and then cooled to room temperature. Subsequently, the sample was heated to 950 °C with a heating rate of 10 °C min^{-1} under 10 vol% H_2/Ar (30 mL min^{-1}).

CO chemisorption was performed on Micromeritics Autochem 2920 instrument with a thermal conductivity detector (TCD), In a typical run for CO chemisorption, 100 mg of the catalyst was pre-reduced at 400 °C in 10 vol% H_2 + 90 vol% N_2 (30 mL min^{-1}) for 1h, and then it was purged with pure He (30 mL min^{-1}) for another 1h. After the sample was cooled to 30 °C in pure He, 5 vol% CO + 95 vol% He pulses were introduced. The Pt dispersion and the number of Pt monometallic sites were calculated on the basis of Pt/CO atomic ratio with 1:1 stoichiometry.[2-4] The number of Pt-BFA interfacial sites was calculated via the following equation: Quantity of the surface Pt-BFA interfacial sites = The number of total surfacial Pt sites – the number of metallic Pt sites (determined by actual CO uptake in CO chemisorption).[3, 5] The number of total surfacial Pt sites was estimated based on assumption of a spheroidal nanoparticle of platinum. The radius of Pt particles was obtained from HAADF-STEM analysis. Firstly, we estimated the number of Pt atoms in one Pt nanoparticles, which equal to total volume of Pt particle divide by volume of single Pt atom (N1); Secondly, we calculated the number of atoms below the surface layer of the sphere (N2), the radius of which equal to the nanoparticle radius minus one diameter of the Pt atom (0.278 nm). Third, the number of surfacial Pt sites in one Pt particle = N1 - N2. Fourth, the number of total number of Pt sites= $(N1 - N2) \times \frac{mass\ of\ Pt\ in\ 1\ g\ of\ sample}{mass\ of\ Pt\ in\ one\ Pt\ particle}$.

In situ diffuse reflectance infrared Fourier transform spectroscopy (in situ DRIFTS) characterization was carried out on a Thermo Scientific Nicolet IS50, equipped with a MCT detector, and operated at a resolution of 4 cm^{-1}. *(1) CO adsorption DRIFTS*: (i) For Pt/BFA-xH (x = 4, 5, 6, 7, 8) and Pt/BFA-8H 4h samples, the samples were cooled to the 20 °C under Ar atmosphere after reduction. (ii) For Pt/BFA-8HO, Pt/BFA-8O and Pt/BFA-8H, the samples except Pt/BFA-8H were reduced at 400 °C for 0.5h under H_2 atmosphere. Then the gas changed from H_2 to Ar and the temperature was cooled to 20 °C. The background spectrum was then recorded, followed by introducing 1 vol% CO/Ar (15 mL min^{-1}). After that, the temperature was raised to 40, 60, 80 and 100 °C. The data was collected with time on stream. (2) In situ DRIFTS under sequential CO → O_2 → CO+O_2 atmospheres: The samples except Pt/BFA-8H were reduced at 400 °C for 0.5h under H_2 atmosphere. Then the gas changed from H_2 to Ar and the temperature was cooled to 50 °C. The background spectrum was then recorded. 1 vol% CO/Ar was first passed through the chamber for 15 min, followed by purging with Ar for another 15 min. Then 1 vol% O_2/Ar was introduced for 15 min and then the gas composition was changed to 1 vol% CO +1 vol% O_2 balanced with Ar for 15 min. The data was collected with time on stream. *(3) C_3H_8 adsorption DRIFTS*: the samples except Pt/BFA-8H was pre-reduced at 400 °C for 1h and then cooled to 30 °C in Ar atmosphere. After the recording of back ground spectrum, 0.2 vol% C_3H_8 (balanced with Ar) was introduced. All DRIFTS spectra were obtained under steady-state conditions. *(4)* In situ DRIFTS under sequential C_3H_8 → O_2 → C_3H_8+O_2 atmospheres: The samples except Pt/BFA-8H were reduced at 400 °C for 0.5h under H_2 atmosphere. Then the gas changed from H_2 to Ar and the temperature was cooled to 250 °C. The background spectrum was then recorded. 0.2 vol% C_3H_8/Ar was first passed through the chamber for 15 min, followed by purging with purging with Ar for another 15 min. Then 2 vol% O_2/Ar was introduced for 15 min and then the gas composition was changed to 0.2 vol% C_3H_8 + 2 vol-%_–O_2 + 97.8 vol-% Ar for 15 min. The data was collected with time on stream.

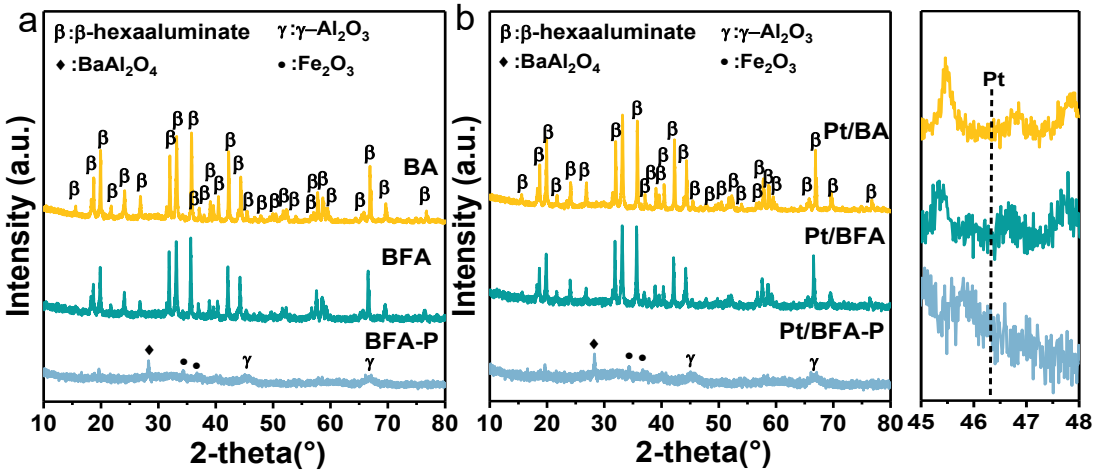

Fig. S1 XRD patterns over (a) supports and (b) catalysts.

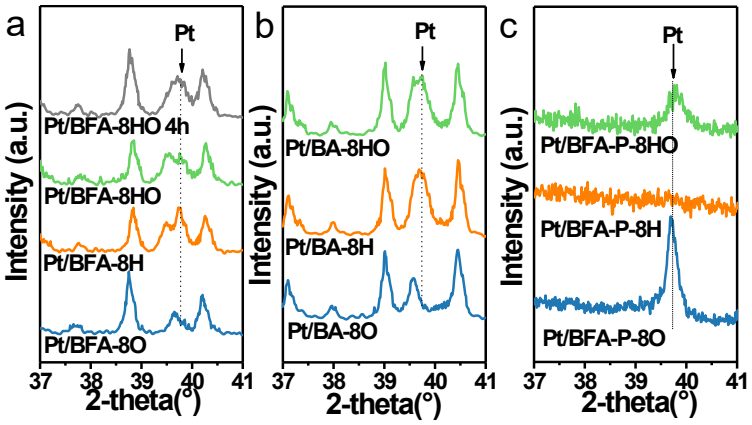

Fig. S2 XRD patterns from 37° to 41° for (a) Pt/BFA, (b) Pt/BA and (c) Pt/BFA-P calcined under different atmospheres.

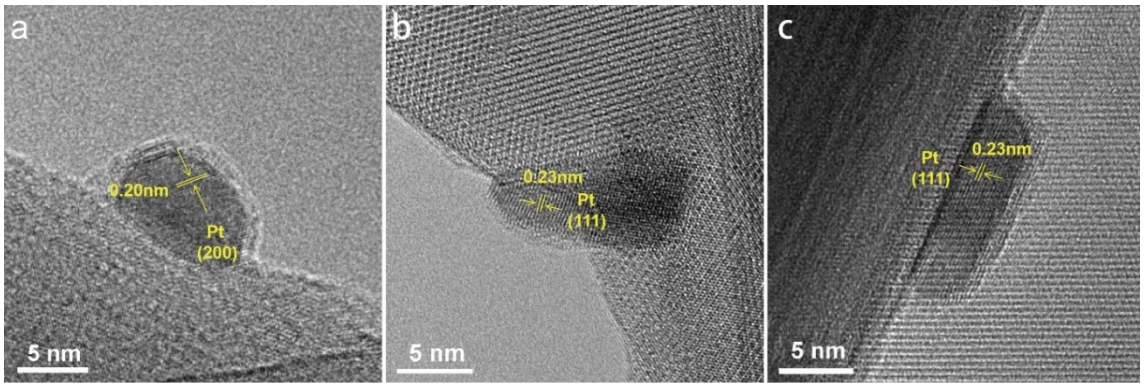

Fig. S3 HRTEM images of Pt/BFA-8H.

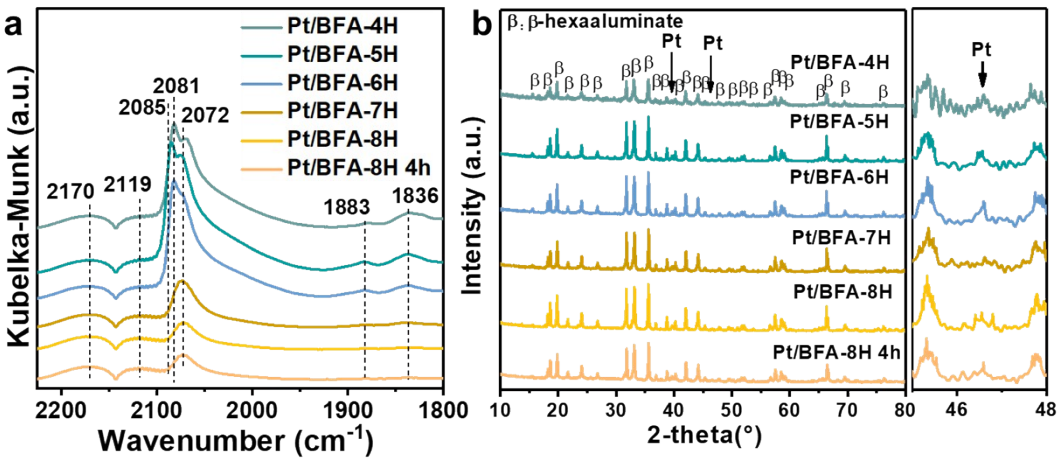

Fig. S4 (a) CO DRIFTS of Pt/BFA reduced at various temperatures and time; (b) XRD patterns and its enlargement for Pt/BFA reduced at different temperatures.

The SMSI phenomenon on Pt/BFA was further studied via in situ CO adsorption DRIFTS (Fig. S4a). The peak at 2072 cm^{-1} and 2081-2085 cm^{-1} is attributed to the linear adsorption of CO on Pt^0 sites and partially oxidized Pt species ($Pt^{\delta+}$), respectively.[6, 7] In addition, peaks at around 1883 cm^{-1} and 1836 cm^{-1} can be assigned to CO bridge-bonded to platinum particles.[6-8] As shown, CO linear-bonded peaks were strong and kept nearly unchanged at reduction temperatures of 400-600 °C. When the reduction temperature was higher than 700 °C, intensities of all adsorbed CO peaks rapidly decreased and the peaks at 2081-2085 cm^{-1}, 1883 cm^{-1} and 1836 cm^{-1} were nearly absent. These facts suggest the cover of BFA support on Pt particles.[2, 7, 9-12] Furthermore, combined with the indistinctive change on intensities of XRD peaks assigned to Pt crystal phase for samples calcined under different temperatures (Fig. S4b), the encapsulation of Pt metal by BFA support overlayers is confirmed. The CO adsorption peaks do not disappear with further increasing the reduction temperatures or prolonging the calcination time. This could be due to the amorphous structure of coating layer observed from Fig. 2b and S3, which enables the permeation of molecules such as CO to active Pt sites.[13]

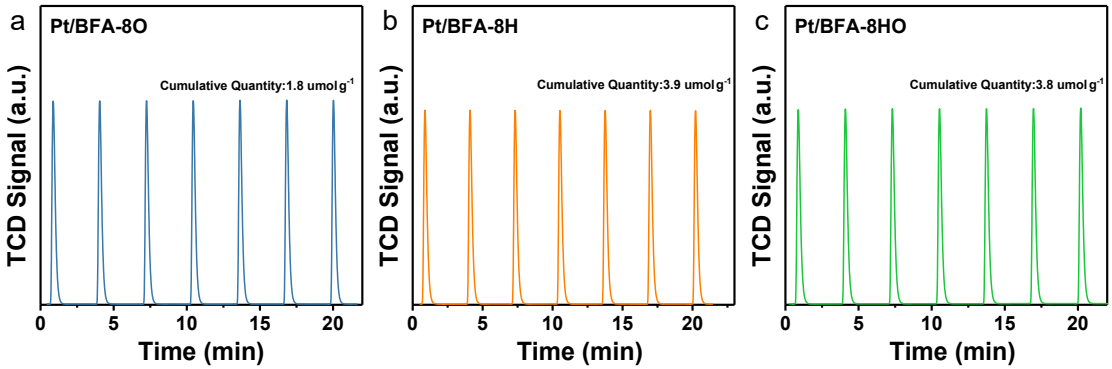

Fig. S5 The CO chemisorption spectrum at 30 °C over (a) Pt/BFA-8O, (b) Pt/BFA-8H and (c) Pt/BFA-8HO.

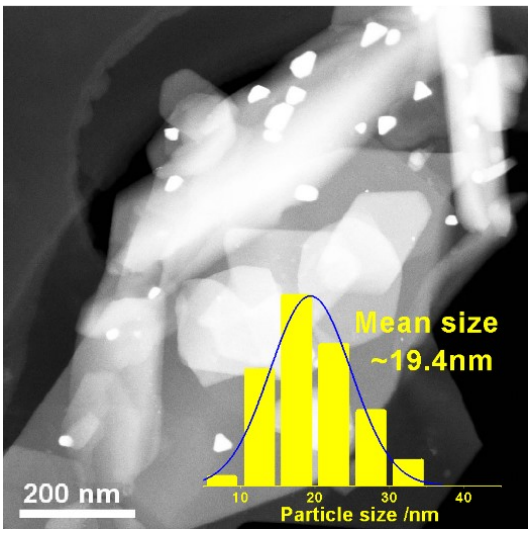

Fig. S6 HAADF-STEM images (the inset shows particle size distribution) of Pt/BFA-8HO 4h.

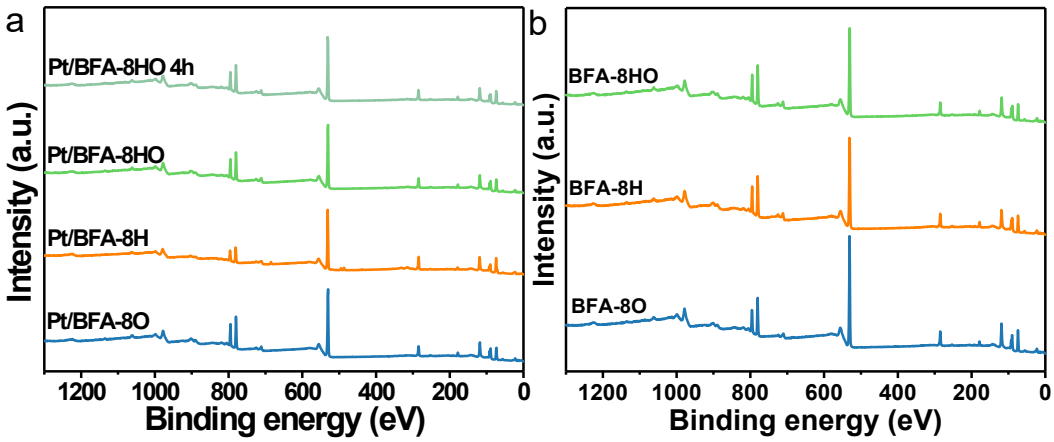

Fig. S7 The full spectra of XPS over (a) Pt/BFA and (b) BFA treated under different conditions.

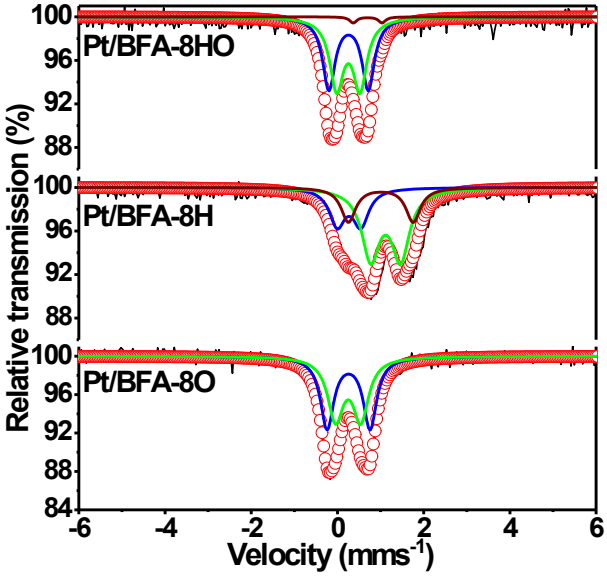

Fig. S8 ^{57}Fe Mössbauer spectra of Pt/BFA treated under different atmospheres at 800 °C.

As shown in Fig. S8 and Table S3, the reductive treatment resulted in the generation of Fe^{2+} for Pt/BFA-8H in comparison to BFA support with framework Fe^{3+} in Al(2) and Al(5) sites reported in our previous work.[14] The following oxidative calcination led to the full oxidation of reduced Fe cations over Pt/BFA-8HO and Pt/BFA-8HO 4h, the occupancies of Fe^{3+} ions in which were similar to Pt/BFA-8O and BFA.

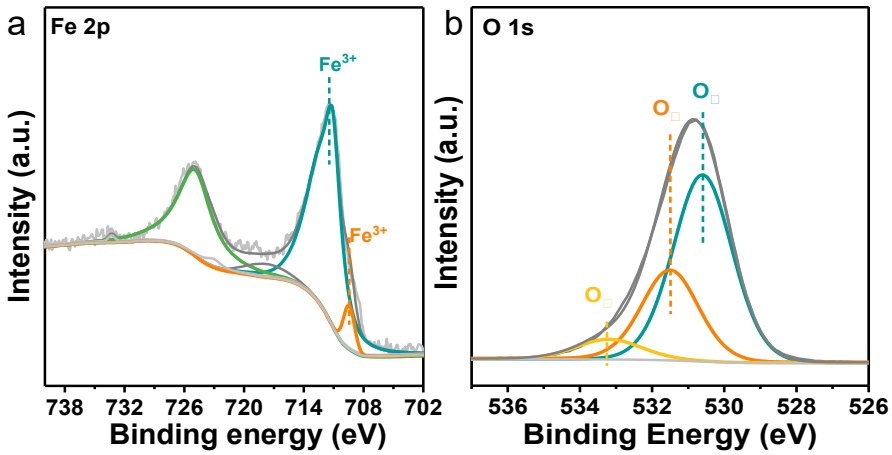

Fig. S9 (a) Fe 2p and (b) O 1s XPS spectra over Pt/BFA-8HO 4h catalyst.

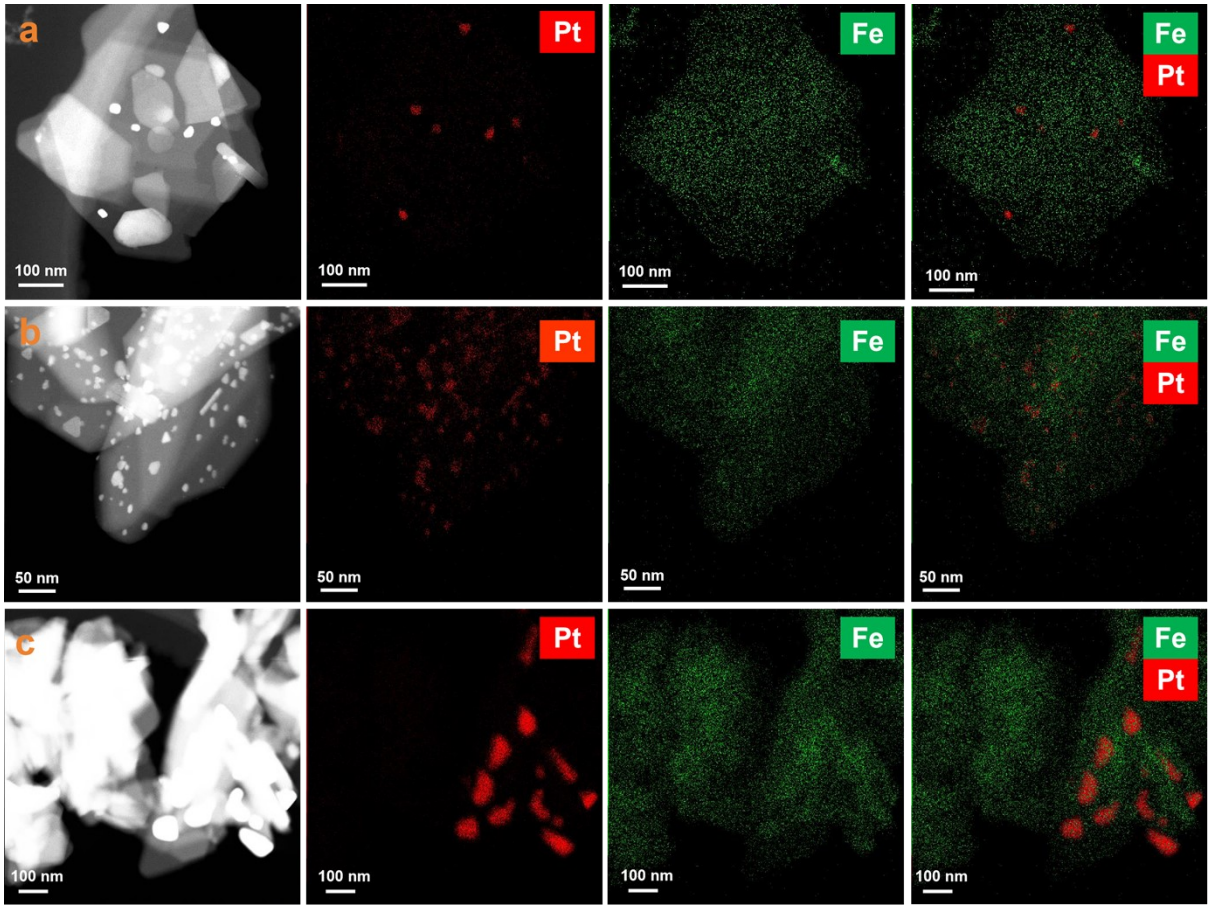

Fig. S10 HAADF-STEM images and corresponding EDS elemental mapping of (a) Pt/BFA-8HO, (b) Pt/BFA-8H and (c) Pt/BFA-8O.

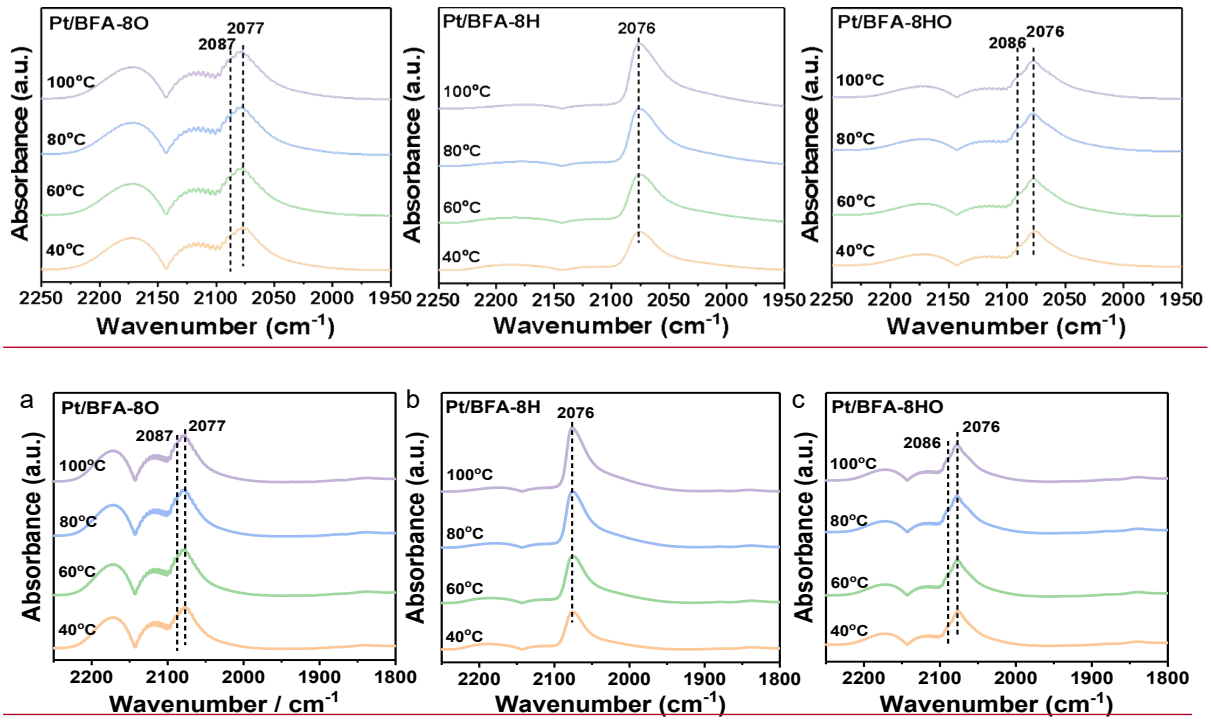

Fig. S11 Temperature-dependent CO adsorption DRIFTS measurement on Pt/BFA-8O, Pt/BFA-8H and Pt/BFA-8HO. Before measurement, the Pt/BFA-8O and Pt/BFA-8HO catalysts were pre-reduced at 400 °C for 0.5 h.

As displayed, strong vibration peak around 2076 cm^{-1} and relatively weak band at around 2086 cm^{-1} is attributed to the linear adsorption of CO on Pt^0 sites and partially oxidized Pt species ($Pt^{\delta+}$), respectively.[6, 7] As reported, the $Pt^{\delta+}$ species over Pt/BFA-8HO and Pt/BFA-8O would probably be associated with the Pt-hexaaluminate interface.[7] Whereas, the band at 2086 cm^{-1} was absent for Pt/BFA-8H, which would be ascribed to the encapsulation of BFA support on Pt nanoparticles.[12]

When the temperature increased from 40 to 100 °C, there was no red-shift of vibration frequency for all samples, suggesting that the dipole-dipole coupling effect can be excluded and the signal of adsorbed CO on Pt^0 could effectively reflect the chemical state of Pt metal.[15-17] Therefore, the similar peak position at 40 °C suggests the analogous oxidation state of Pt particles among Pt/BFA-8O, Pt/BFA-8H and Pt/BFA-8HO samples.

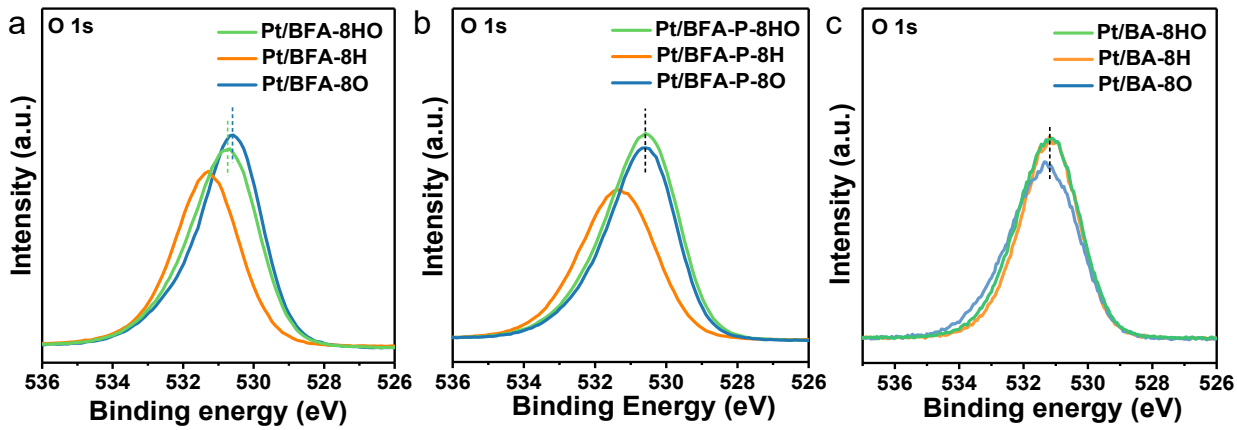

Fig. S12 O 1s XPS spectra over Pt/BFA, Pt/BFA-P and Pt/BA treated under different atmosphere.

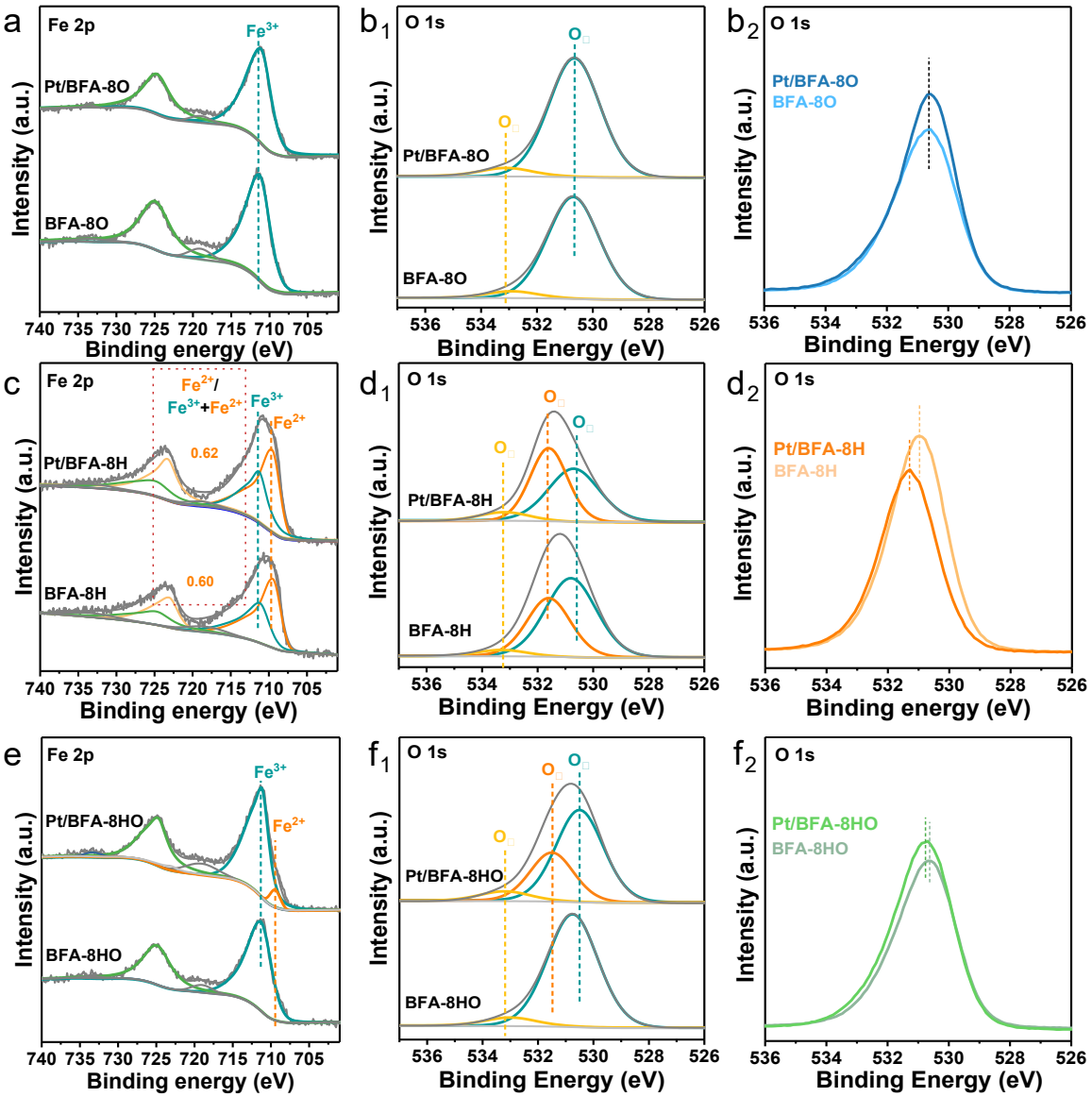

Fig. S13 XPS spectra of (a, c, e) Fe 2p and (b, d, f) O 1s for BFA and Pt/BFA treated under different atmospheres at 800 °C.

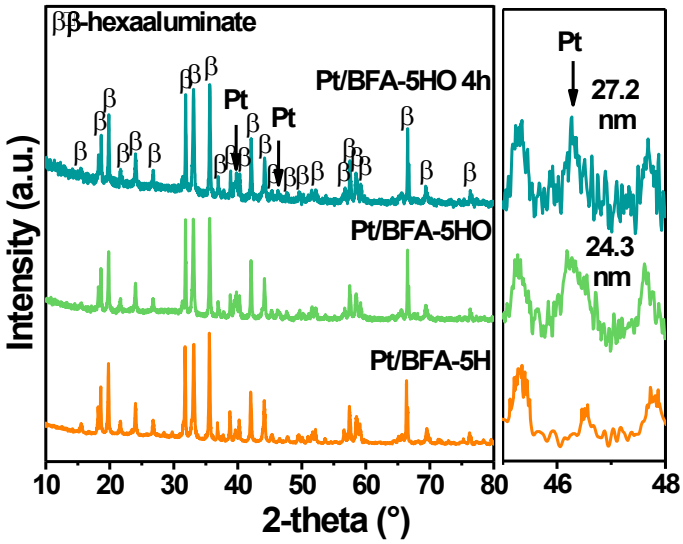

Fig. S14 XRD patterns and its enlargement for Pt/BFA reduced at 500 °C and followed by oxidative calcination at 800 °C.

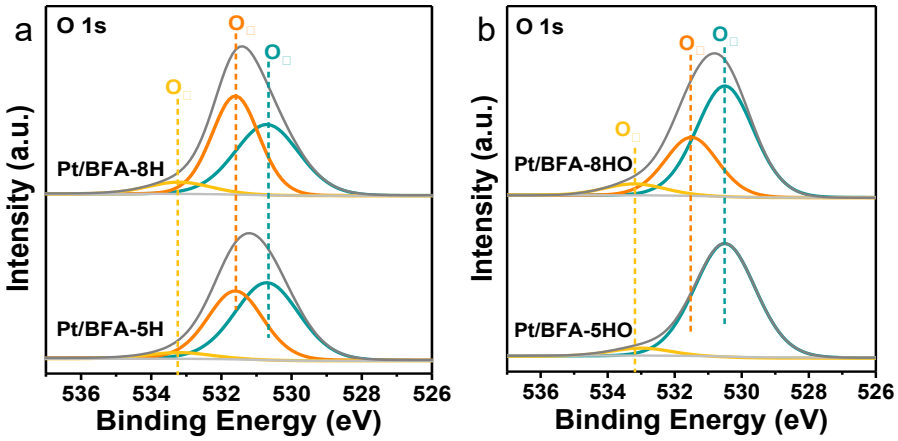

Fig. S15 O 1s XPS spectra for (a) Pt/BFA-xH and (b) Pt/BFA-xHO treated under different atmospheres at 800 °C (x=5;8).

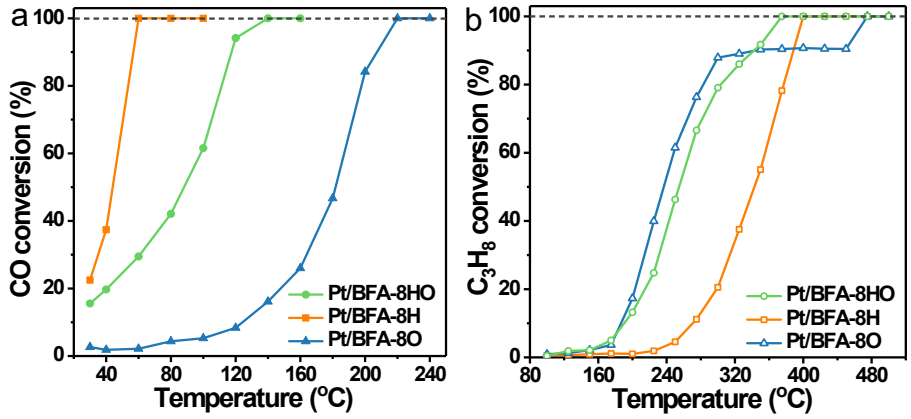

Fig. S16 (a) CO conversion and (b) C_3H_8 conversion as a function of temperature over different catalysts.

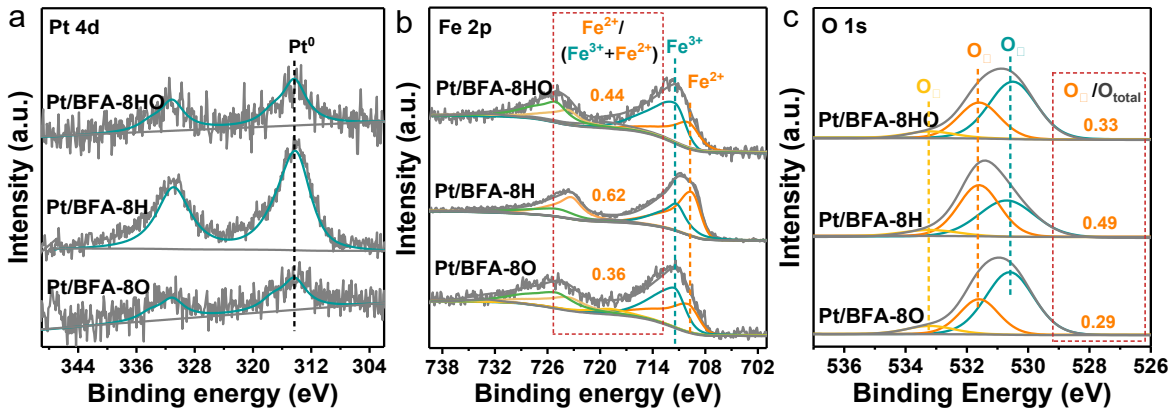

Fig. S17 XPS spectra of (a) Pt 4d, (b) Fe 2p and (c) O 1s for Pt/BFA -8HO, Pt/BFA-8O reduced at 400 °C for 1h and Pt/BFA-8H.

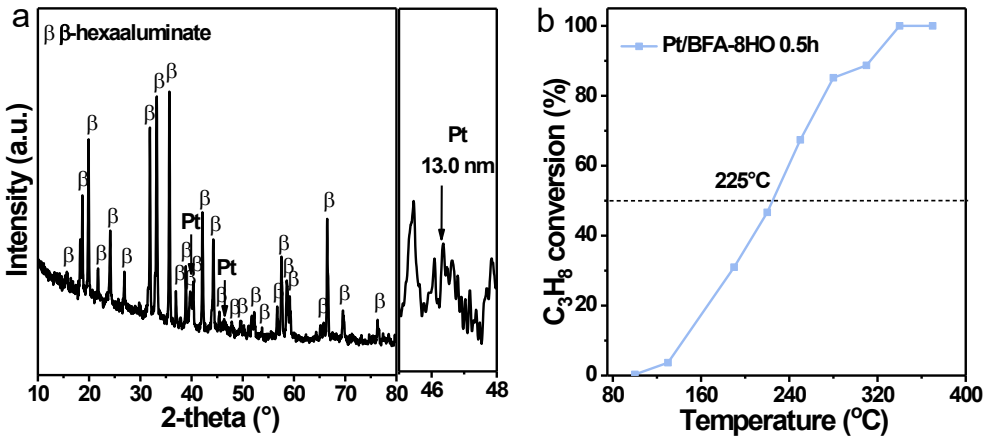

Fig. S18 (a) XRD patterns and its enlargement for Pt/BFA-8HO 0.5h; (b) C_3H_8 conversion as a function of temperature over Pt/BFA-8HO 0.5h. Reaction conditions: 0.2 vol % C_3H_8 + 2 vol % O_2 + 97.8 vol % Ar. Before the test, the sample was reduced at 400 °C for 1h.

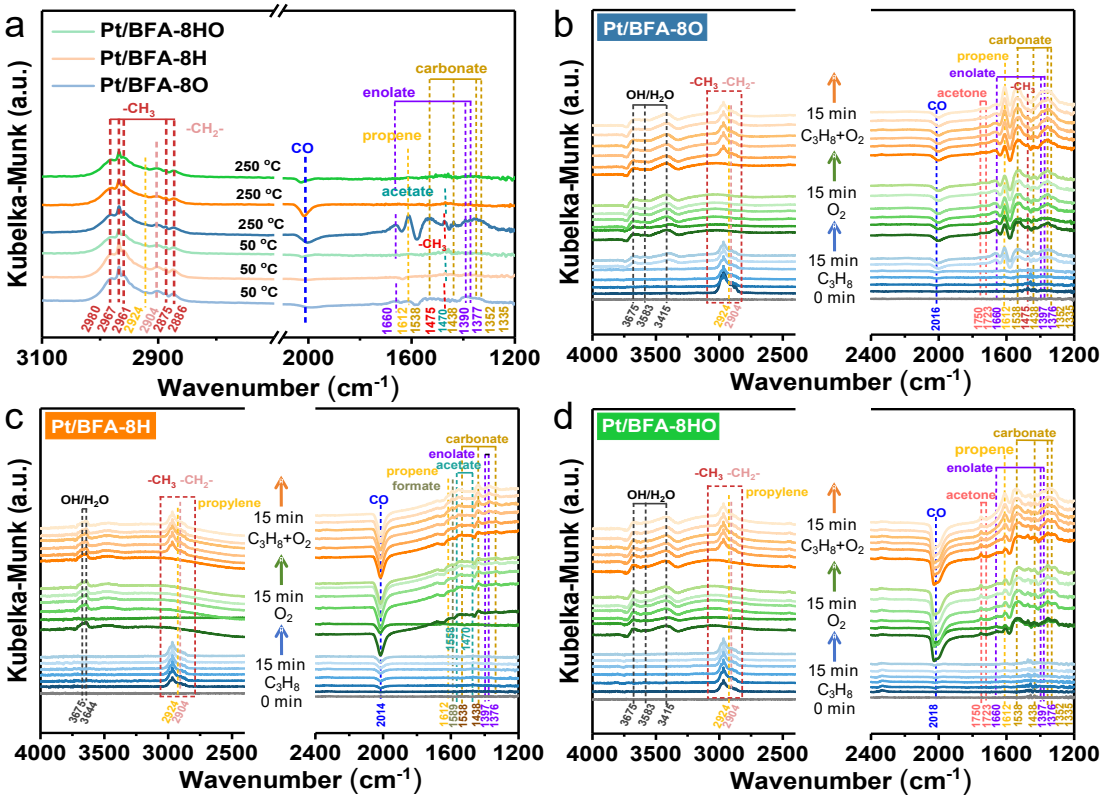

Fig. S19 In situ DRIFT spectra over Pt/BFA-8O, Pt/BFA-8H, and Pt/BFA-8HO catalysts under conditions of (a) C_3H_8 adsorption (0.2 vol% C_3H_8 + 99.8 vol% Ar) at 30 °C and 250 °C. In-situ DRIFT spectra of C_3H_8 oxidation over (b) Pt/BFA-8O, (c) Pt/BFA-8H and (d) Pt/BFA-8HO catalysts at 250 °C. Note: The catalyst was first exposed to 0.2 vol% C_3H_8 for 15 min until the C_3H_8 adsorption was saturated. After purging by Ar for 15 min, 2 vol% O_2 and 0.2 vol% C_3H_8 +2 vol%O_2 was introduced and the DRIFTS spectra were recorded.

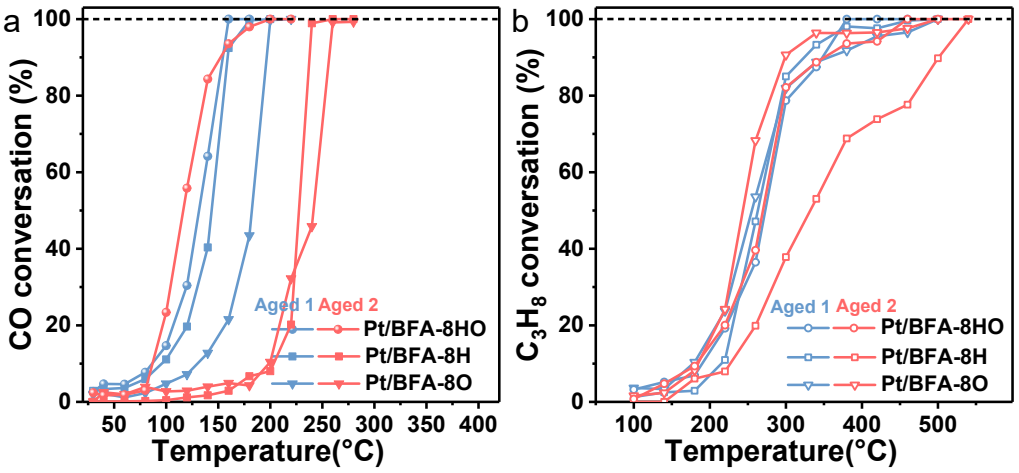

Fig. S20 The (a) CO conversion and (b) C_3H_8 conversion as a function of temperature over Pt/BFA-8H, Pt/BFA-8HO and Pt/BFA-8O catalysts after hydrothermal aging.

Table S1. Characteristic and reaction results of samples treated under different conditions.

Catalysts	d_{Pt1}[a] (nm)	d_{Pt2}[b] (nm)	Surface area (m^2g^{-1})	Cumulative Quantity of CO [b] (umol g^{-1})	Pt-BFA interfacial sites[c] (umol g^{-1})	Fe^{2+}/ (Fe^{2+}+Fe^{3+}) [d]	O_{II}/ O_{total}	CO oxidation T_{50}(°C) [e]	C_3H_8 Oxidation T_{50}(°C)[e]
Pt/BFA-8O	25.9	62.3	13.5	1.8	0	-	-	182	234
Pt/BFA-8H	-	28.2	13.8	3.9	7.0	0.62	0.49	44	339
Pt/BFA-8HO	16.7	29.0	14.2	3.8	1.7	0.05	0.23	88	254
Pt/BA-8O	24.2	-	13.5	-	-	-	-	231	
Pt/BA-8H	-	-	13.5	-	-	-	-	146	
Pt/BA-8HO	22.7	-	12.9	-	-	-	-	266	
Pt/BFA-P-8O	35.6	-	113.6	-	-	-	-	173	
Pt/BFA-P-8H	-	-	105.2	-	-	-	0.43	108	
Pt/BFA-P-8HO	21.2	-	92.6	-	-	-	-	169	

Pt/BFA-8HO 0.5h	13.0	-	-	-	-	-	-	-	225
Pt/BFA-8HO 4h	17.5	-	-	-	-	0.05	0.25	93	264
Pt/BFA-5H	-	-	-	-	-	0.53	0.37	-	-
Pt/BFA-5HO	24.3	-	-	-	-	-	-	-	-
Pt/BFA-5HO 4h	27.2	-	-	-	-	-	-	-	-

[a]. Estimated according to the Scherrer equation using the full width at half maximum (FWHM) of Pt (200) peak.

[b]. Calculated based on the CO chemisorption data (CO/Pt=1/1) at 30°C.

[c]. The number of Pt-BFA interfacial sites was calculated via the following equation: Quantity of the surface Pt-BFA interfacial sites = The number of total surfacial Pt sites – the number of metallic Pt sites (determined by actual CO uptake in CO chemisorption).

[d]. obtained from XPS results.

[e]. T_{50} represents the temperature for 50% CO or C_3H_8 conversion.

Table S2. XPS analysis of Fe 2p binding energy over BFA, Pt/BFA samples treated under different conditions.

Catalysts	Fe(eV)							
	Fe^0 $2p_{3/2}$	Fe^{2+} $2p_{3/2}$	Fe^{3+} $2p_{3/2}$	Satellite	Fe^0 $2p_{1/2}$	Fe^{2+} $2p_{1/2}$	Fe^{3+} $2p_{1/2}$	Satellite
Pt/BFA-8O	-	-	711.0	719.0	-	-	724.7	733.3
Pt/BFA-8H	-	709.6	711.3	718.8	-	723.3	724.9	733.3
Pt/BFA-8HO	-	709.5	711.2	719.0	-	723.1	724.8	733.3
Pt/BFA-8HO 4h	-	709.5	711.2	717.8	-	723.1	724.9	733.3
Pt/BFA-P-8H	706.8	709.8	711.2	718.2	720.4	723.4	724.6	733.3
Pt/BFA-P-8HO	-	-	711.0	719.3	-	-	724.3	733.3
Pt/BFA-P-8O	-	-	711.0	720.0	-	-	724.6	733.0
Pt/BFA-5H	-	709.9	711.3	719.0	-	723.6	724.9	733.3
Pt/BFA-5HO	-	-	711.0	719.0	-	-	724.7	733.3
BFA-8O	-	-	711.3	719.0	-	-	724.9	733.3
BFA-8H	-	709.5	711.2	718.4	-	723.1	724.8	733.3
BFA-8HO	-	-	711.3	719.0	-	-	724.9	733.3

Table S3. ^{57}Fe Mössbauer parameters of Pt/BFA treated in different atmosphere.

Catalysts	IS[b] (mm s^{-1})	QS[c] (mm s^{-1})	H[d] (KOe)	A[e]	Blocks	Assignment
BFA[a]	0.21	0.60	-	51	Spinel	Fe^{3+} in Al(2) sites
	0.23	1.01	-	49	Mirror	Fe^{3+} in Al(5) sites
Pt/BFA-8O	0.25	0.59	-	50	Spinel	Fe^{3+} in Al(2) sites
	0.26	1.00	-	50	Mirror	Fe^{3+} in Al(5) sites
Pt/BFA-8H	0.27	0.55	-	25	Spinel	Fe^{3+} in Al(2) sites
	1.12	0.69	-	53	-	Fe^{2+}
	1.01	1.50	-	22	-	Fe^{2+}
Pt/BFA-8HO	0.25	0.51	-	44	Spinel	Fe^{3+} in Al(2) sites
	0.26	0.89	--	56	Mirror	Fe^{3+} in Al(5) sites
Pt/BFA-8HO 4h	0.25	0.55	-	44	Spinel	Fe^{3+} in Al(2) sites
	0.26	0.90	-	56	Mirror	Fe^{3+} in Al(5) sites

[a] According to our previous work [*J. Energy Chem. 2019,29, 50–57*].

[b] Isomer shift relative to α-Fe.

[c] Quadrupole splitting.

[d] Magnetic field

[e] Relative area: uncertainty is ±5% of reported value.

[f] Octahedral

[g] Tetrahedral

Table S4. XPS analysis of O 1s signals over BFA, Pt/BFA treated under different conditions.

Catalysts	O 1s(eV)		
	O_I	O_{II}	O_{III}
Pt/BFA-8O	530.6	-	533.2
Pt/BFA-8H	530.6	531.6	533.2
Pt/BFA-8HO	530.6	531.5	533.2
Pt/BFA-8HO 4h	530.6	531.6	533.2
Pt/BA-8O	530.2	-	533.1
Pt/BA-8H	530.2	-	533.1
Pt/BA-8HO	530.2	-	533.1
Pt/BFA-P-8O	530.6	-	533.2
Pt/BFA-P-8H	530.6	531.6	533.2
Pt/BFA-P-8HO	530.6	-	533.2
Pt/BFA-5H	530.6	531.6	533.2
Pt/BFA-5HO	530.6	-	533.2
BFA-8O	530.6	-	533.2
BFA-8H	530.6	531.6	533.2
BFA-8HO	530.6	-	533.2

Table S5. H_2-TPR results of samples.

Catalysts	Peak temperature (°C)	
BFA	-	490
Pt/BFA	144	456
BA	-	-
Pt/BA	-	-

Table S6. Kinetic parameters of CO oxidation (T=40 °C) and C_3H_8 oxidation (T=220 °C) over the Pt/BFA-8O, Pt/BFA-8H and Pt/BFA-8HO catalysts.

Catalyst	$r=k[P_{CO}]^a[P_{O2}]^b$ (CO oxidation)				$r=k[P_{C3H8}]^c[P_{O2}]^d$ (C_3H_8 oxidation)			
	k ($\times10^{-5}$)	a	b	Ea(KJ • mol^{-1})	k ($\times10^{-5}$)	c	d	Ea(KJ • mol^{-1})
Pt/BFA-8O	2.86	0.03±0.01	0.98±0.01	67.9±2.1	5.70	0.89±0.02	-0.12±0.02	42.6±3.2
Pt/BFA-8H	7.70	0.07±0.02	1.01±0.02	28.8±3.3	3.75	0.99±0.02	-0.10±0.01	74.1±1.4
Pt/BFA-8HO	5.83	0.06±0.01	0.99±0.01	44.5±1.8	5.16	1.02±0.01	-0.09±0.01	41.5±2.5

Table S7. Frequencies of functional groups present on the Pt/BFA-8H, Pt/BFA-8HO and Pt/BFA-8O catalysts analyzed by DRIFTS about propane adsorption and oxidation.

Assignment	Vibrational mode	Infrared band wavenumber (cm^{-1})			Reference
		Pt/BFA-8H	Pt/BFA-8HO	Pt/BFA-8O	
H_2O	-OH	3200-3800	3200-3800	3200-3800	18-20
Propane	$-CH_3$	2980, 2967, 2961, 2875, 2886			3, 21
	$-CH_2-$	2904			
CO		2014	2018	2016	7, 22
Acetone	ν(C=O)	-	1750, 1723	1750, 1723	21, 23
Propylene	δ(CH)	2924			21, 24
	ν(C=C)	1612			
Formate	$\nu_{as}(COO)$	1589	-	-	25
Methoxy	$\delta_{as}(CH_3)$	-	-	1475	25
Acetate	$\nu_{as}(COO)$	1558	-	-	21, 25
	$\nu_s(COO)$	1470	-	-	
Enolate	$\nu_{as}(CH_2=CH-O)$	-	1660	1660	23, 26
	$\nu_s(CH_2=CH-O)$	1397			
	δ (CH)	1376			
Carbonate	-	1538, 1438, 1352, 1335			3, 7, 21, 27

References:

1. B. Hong, J.-X. Liang, X. Sun, M. Tian, F. Huang, Y. Zheng, J. Lin, L. Li, Y. Zhou and X. Wang, *ACS Catal.*, 2021, **11**, 5709-5717.
2. I. Ro, I. B. Aragao, J. P. Chada, Y. Liu, K. R. Rivera-Dones, M. R. Ball, D. Zanchet, J. A. Dumesic and G. W. Huber, *J. Catal.*, 2018, **358**, 19-26.
3. P.-P. Zhao, J. Chen, H.-B. Yu, B.-H. Cen, W.-Y. Wang, M.-F. Luo and J.-Q. Lu, *J. Catal.*, 2020, **391**, 80-90.
4. I. Ro, C. Sener, T. M. Stadelman, M. R. Ball, J. M. Venegas, S. P. Burt, I. Hermans, J. A. Dumesic and G. W. Huber, *J. Catal.*, 2016, **344**, 784-794.
5. R. Carrasquillo-Flores, I. Ro, M. D. Kumbhalkar, S. Burt, C. A. Carrero, A. C. Alba-Rubio, J. T. Miller, I. Hermans, G. W. Huber and J. A. Dumesic, *J. Am. Chem. Soc.*, 2015, **137**, 10317-10325.
6. M. Di, K. Simmance, A. Schaefer, Y. Feng, F. Hemmingsson, M. Skoglundh, T. Bell, D. Thompsett, L. I. Ajakaiye Jensen, S. Blomberg and P.-A. Carlsson, *J. Catal.*, 2022, **409**, 1-11.
7. B. Li, X.-F. Wang, W.-Y. Wang, C.-F. Liu, L.-C. He, M.-F. Luo and J. Chen, *Appl. Catal., A*, 2023, **649**, 118960.
8. X. Liu, S. Jia, M. Yang, Y. Tang, Y. Wen, S. Chu, J. Wang, B. Shan and R. Chen, *Nat. Comm.*, 2020, **11**, 4240.
9. S. Lee, S. Kim, T. Kim, C. Lin, W.-J. Lee, S.-J. Kim, R. J. Gorte and W. Jung, *Catal. Commun.*, 2022, **172**, 106549.
10. K. Shen, S. Lee, O. Kwon, M. Fan, R. J. Gorte and J. M. Vohs, *ACS Catal.*, 2023, **13**, 11144-11152.
11. X. Mao, A. C. Foucher, T. Montini, E. A. Stach, P. Fornasiero and R. J. Gorte, *J. Am. Chem. Soc.*, 2020, **142**, 10373-10382.
12. L. Cao, W. Liu, Q. Luo, R. Yin, B. Wang, J. Weissenrieder, M. Soldemo, H. Yan, Y. Lin, Z. Sun, C. Ma, W. Zhang, S. Chen, H. Wang, Q. Guan, T. Yao, S. Wei, J. Yang and J. Lu, *Nature*, 2019, **565**, 631-635.
13. F. Huang, M. Tian, Y. Zhu, X. Wang, A. Wang, L. Li, J. Lin and J. Wang, *J. Energy Chem.*, 2019, **29**, 50-57.
14. K. Shen, J.-P. Lin, Q. Xia, L. Dai, G.-J. Zhou, Y.-L. Guo, G.-Z. Lu and W.-C. Zhan, *Rare Metals*, 2018, **38**, 107-114.
15. *Springer Handbook of Advanced Catalyst Characterization*, 2023.
16. T. Wang, J.-Y. Xing, A.-P. Jia, C. Tang, Y.-J. Wang, M.-F. Luo and J.-Q. Lu, *J. Catal.*, 2020, **382**, 192-203.
17. K. Ding, A. Gulec, A. M. Johnson, N. M. Schweitzer, G. D. Stucky, L. D. Marks and P. C. Stair, *Science*, 2015, **350**, 189-192.
18. K. Murata, J. Ohyama, Y. Yamamoto, S. Arai and A. Satsuma, *ACS Catal.*, 2020, **10**, 8149-8156.
19. Y. An, S.-Y. Chen, B. Wang, L. Zhou, G. Hao, Y. Wang, J. Chen, C.-K. Tsung, Z. Liu and L.-Y. Chou, *J. Mater. Chem. A*, 2023, **11**, 16838-16845.
20. J. Saavedra, H. A. Doan, C. J. Pursell, L. C. Grabow and B. D. Chandler, *Science*, 2014, **345**, 1599−1602.
21. F. He, C. Rao, S. Tao, L. Sun, T. Yi, H. Wang, B. Hu, X. Yang and Y. Zhang, *ACS Appl. Nano Mater.*, 2024, **7**, 11609-11620.
22. J. Liu, F. R. Lucci, M. Yang, S. Lee, M. D. Marcinkowski, A. J. Therrien, C. T. Williams, E. C. Sykes and M. Flytzani-Stephanopoulos, *J. Am. Chem. Soc.*, 2016, **138**, 6396-6399.
23. Y. You, A. Xu, Y. Lv, L. Yang, X. Tang, J. Tang, Y. Guo, Y. Cui, W. Zhan, L. Wang, Y. Guo and S. Dai, *Catal. Sci. Technol.*, 2024, **14**, 4058-4067.
24. Y. Shi, J. Li, Q. Wang, S. Yao, Z. Wu, E. Gao, W. Wang, J. Zhu, L. Li and N. Wu, *Sep. Purif. Technol.*, 2024, **328**, 125101.
25. C. P. O'Brien and I. C. Lee, *J. Catal.*, 2017, **347**, 1-8.
26. X.-F. Wang, L.-Y. Xu, C.-H. Wen, D.-D. Li, B. Li, J.-Q. Lu, Q.-H. Yang, M.-F. Luo and J. Chen, *Appl. Catal., B*, 2023, **338**, 123000.
27. C.-F. Liu, X.-F. Wang, C.-H. Wen, B. Li, C. Tang, J.-Q. Lu, M.-F. Luo and J. Chen, *Appl. Surf. Sci.*, 2023, **617**, 156572.